11

Overview of Rydberg Atom-Based Sensors/Receivers for the Measurement of Electric Fields, Power, Voltage, and Modulated Signals

Christopher L. Holloway, Matthew T. Simons, Alexandra B. Artusio-Glimpse, and Joshua A. Gordon

U.S. Department of Commerce, Boulder Laboratories, National Institute of Standards and Technology (NIST), Boulder, CO, USA

11.1 Introduction

Guglielmo Marconi performed the first wireless radio transmission measurements in 1895 when he sent and received the first radio signals in Italy. His efforts culminated in 1902 with the first transatlantic transmission. This work was due in part to the efforts of Nikola Tesla and others. While Marconi is widely credited for these first experiments, some authors also give credit to others [1–3].

Prior to radio, we can look even earlier to give tribute to the "truly" first propagation experiments. In 1887, Heinrich R. Hertz was the first to perform experiments to confirm the hypothesis laid out by Maxwell's equations [4]; that is, the equivalence of light and electromagnetic propagation. The research of Maxwell and Hertz is the single most influential work that started the field of electromagnetic theory, leading to today's numerous applications of wireless electromagnetic wave propagation ranging from biomedical imaging to the telecommunication revolution.

Since these first radio wave propagation experiments, individuals have needed to predict and measure an electric (E) field. As such, a relentless pursuit to acquire accurate and direct measurements of E-field began. At the core of all electromagnetic measurements are calibrated probes and antennas. The conventional probe or antenna relies on currents flowing (via conducting electrons) on some type of metallic structure, see Figure 11.1a. To make accurate measurements, a calibration of the probe or antenna is required. Calibrating E-field probes requires a complex and indirect traceability path and presents a chicken-or-egg dilemma. To calibrate a probe, one must place the probe (sensor) in a "known" field. However, to know the field we need a calibrated probe.

One of the keys to developing new science and technologies is to have sound metrological tools and techniques. Whenever possible, we would like these metrological techniques to make absolute measurements of the physical quantity of interest. A stated goal of international metrology organizations is to make all measurements directly traceable to the International System of Units (SI) [5–7]. Measurements based on atoms provide one direct SI traceability path and enable absolute measurements of physical quantities. Measurement standards based on atoms have been used for a number of years for a wide range of measurements: most notable are time (s), frequency (Hz), and length (m). There is a need to extend these atom-based techniques to other physical quantities, such as E-fields. E-field measurements based on the atom allow a simple and direct traceability path and eliminate the chicken-and-egg dilemma by separating the calibration of the probe from the calibration of the field.

Antenna and Array Technologies for Future Wireless Ecosystems, First Edition.
Edited by Y. Jay Guo and Richard W. Ziolkowski.

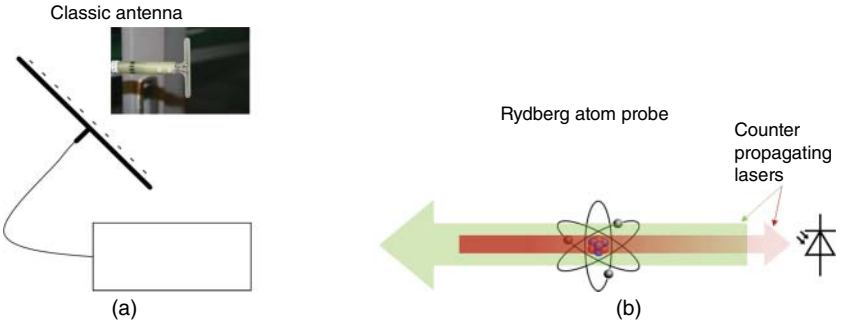

Figure 11.1 Sensor types. (a) Conventional sensors utilize free electrons flowing on metallic structure. (b) Rydberg atom-based sensors utilize atom-bound electrons.

Rydberg atoms provide a pathway to E-field measurements that are traceable to the SI. Rydberg atoms are atoms with one or more electrons excited to a very high principal quantum number n [8]. These atoms have several useful properties that scale as n. In particular, their dipole moments are exceptionally large, scaling with n^2. These large dipole moments make Rydberg atoms sensitive to E-fields and useful for field sensing. In effect, the Rydberg atoms act as the probe and/or antenna as illustrated in Figure 11.1. In this approach, the conventional probe shown in Figure 11.1a is replaced with a glass cell containing Rydberg atoms, and by probing the response of the atoms with light, the incident field strength of a modulated signal can be detected. If alkali atoms are used, the interaction between the Rydberg state and the radio frequency (RF) field can be reliably calculated.

Over the last few years, great progress has been made in the development of Rydberg atom-based RF E-field sensors [9–39]. The Rydberg atom-based sensors have been demonstrated to be capable of measuring amplitude, polarization, and phase of the RF field. As such, various applications are beginning to emerge. These include E-field probes traceable to the SI [11, 12, 15], power-sensors [23], spectrum analyzers [35], angle-of-arrival (AoA) sensors [36], ac and dc voltage measurements [40], receivers for modulated communication signals (AM/FM modulated and digital phase modulation signals) [26–31], and even receivers for recording musical instruments [37]. This new atom-based technology has allowed for many interesting and unforeseen applications. Furthermore, these new Rydberg atom-based sensors will be beneficial for 5G and beyond. In fact, they will allow for traceable calibrations of both field strength and power for frequencies above 100 GHz, which is currently not available. In this chapter we give an overview of this fundamentally new approach for the detection of the E-field and modulated signals.

11.2 Electric-Field Strength: EIT (On Resonant and Stark Shift)

In this section, we give the basic measurement approach. The approach utilizes electromagnetically induced transparency (EIT) [19, 41, 42] to determine the change in the atomic spectra of the Rydberg atoms for an applied E-field, where EIT is used to optically read-out the response of the Rydberg atoms to the applied field. These measurements are performed either when the RF field is on resonance with a Rydberg transition (using Autler–Townes (AT) splitting) or off resonance (using AC Stark shifts). One sensor can measure a field from tens of MHz to above 1 THz. Using standard EIT/AT techniques, E-field strength can be routinely measured down to a few mV/cm [10–12, 14]. With optical homodyne [43] or RF heterodyne (a Rydberg atom-based mixer) [33, 34] techniques with EIT, E-field strengths down to 55–700 nV/cm$\sqrt{\text{Hz}}$ have been measured. At the other extreme,

measured field levels of 10 kV/m and higher have been demonstrated. For such strong field level measurements, the AC stark shift approach is used [16–18].

The basic concept uses a vapor of alkali atoms (placed in a glass cell, referred to as a "vapor" cell, see Figure 11.2a) as the active medium for the RF E-field measurement. Rubidium (^{85}Rb) and cesium (^{133}Cs) are the two atomic species that are typically used in the approach. The classic EIT technique involves using two lasers, one laser called the "probe" laser is used to monitor the optical response of the medium in the vapor cell and a second laser called the "coupling" laser is

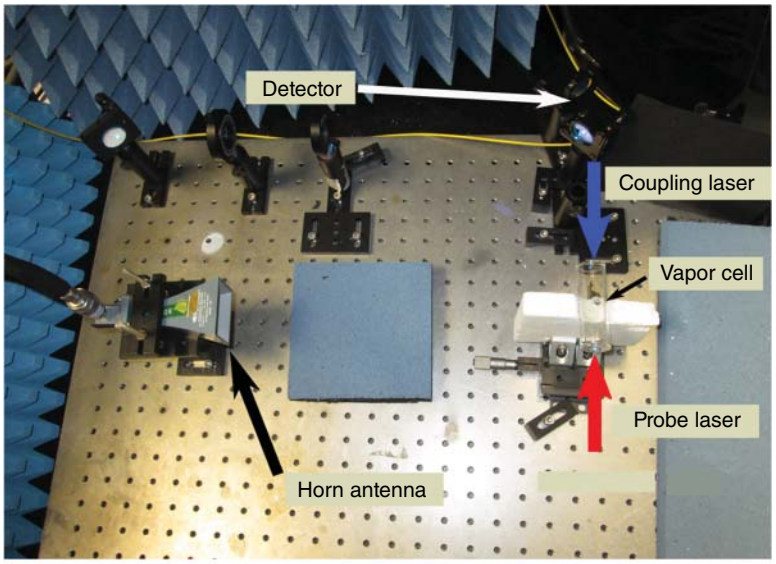

(a)

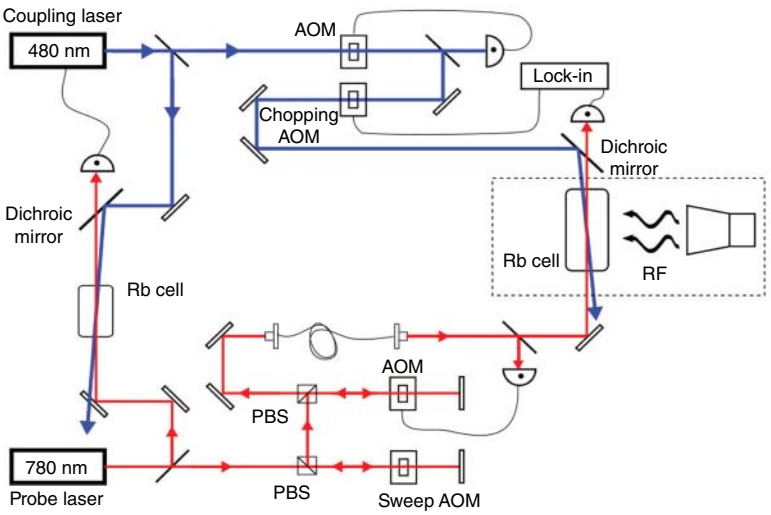

(b)

Figure 11.2 Experimental setup for E-field measurements using EIT. (a) Photo of the system. (b) Block diagram of the system indicating its polarizing beam splitter (PBS) and acousto-optic modulator (AOM). Source: From [12] / with permission from IEEE.

used to establish a coherence in the atomic system. When the RF E-field is applied, it alters the susceptibility of the atomic vapor seen by the probe laser as it propagates through the vapor cell. By detecting the probe light propagating through the cell, i.e. by the change in the susceptibility of the atom population, the RF E-field strength can be determined. We note that three lasers can be used, and the concept is the same with slightly increased complexity [44, 45].

To explain how the three fields (probe, coupling, and RF) interact and influence the atoms, we discuss how the measurement system, diagrammed in Figure 11.2, causes light to be transmitted through the vapor cell when it otherwise would be absorbed by the atoms in the cell. The system nominally consists of an RF source, a lock-in amplifier, a probe laser (780 nm laser), a coupling laser (480 nm laser), a photodetector, and a vapor cell. The alkali atoms ^{85}Rb or ^{133}Cs or sometimes both species are in the vapor cell [22, 28]. In Section 11.8, we look at a compact version of this system where the optical beams are brought to the vapor cell through optical fibers, which allows the vapor cell (the E-field probe) to be more mobile and taken off the optical table.

If we turn on only the probe laser, we find that when it is tuned to a ground state transition of the atoms, they absorb the laser light and little power is detected at the photodetector. For ^{85}Rb, this corresponds to a probe laser wavelength of 780.24 nm, its frequency being 384.231 THz. For ^{133}Cs, this corresponds to a probe laser wavelength of 852.35 nm, its frequency being 351.725 THz. As we scan the probe laser wavelength, the power on the detector changes and shows the so-called Doppler background, which corresponds to the absorption line of the alkali atoms. This spectral response is given in the bottom curve in Figure 11.3a. Here, $\Delta p = \omega_o - \omega_p$ is the frequency detuning of the probe laser, where ω_o is the on-resonance angular frequency of the atom ground state transition and ω_p is the angular frequency of the probe laser. The inverted bell-curve shape of the Doppler background is the typical signal obtained when performing atomic spectroscopy experiments, e.g. studies of absorption and emission properties of atoms. When $\omega_p = \omega_o$, the probe laser is on resonance with the atom ground state transition and the transmitted power through the vapor cell is at a minimum.

Next, we turn on the coupling laser. Typically the coupling laser is aligned to be counter-propagating with respect to the probe laser through the vapor cell. Such a configuration minimizes excessive Doppler broadening of the spectral signatures that arises from the large frequency

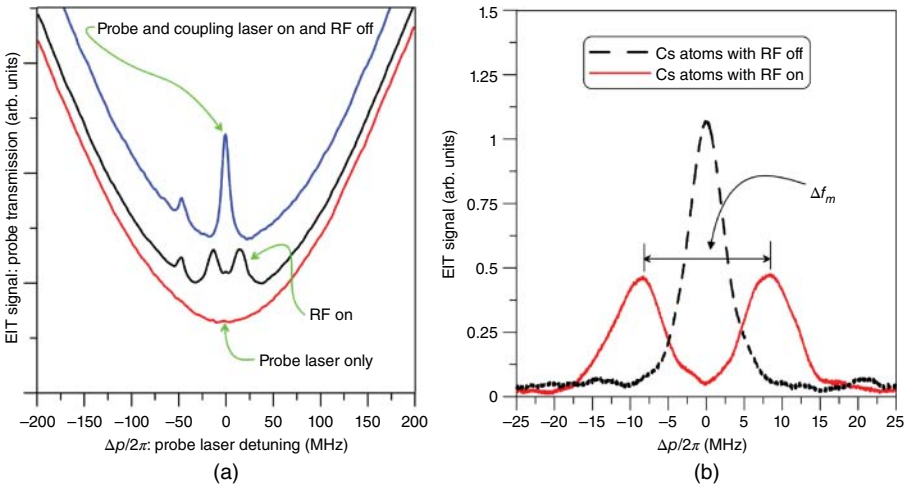

Figure 11.3 EIT signal. (a) With the Doppler background. (b) After the lock-in amplifier is used [12]. Source: From [12] / with permission from IEEE.

difference between the two lasers. The frequency of the coupling laser is tunable according to the measurement requirements, but is typically in the range of 480 nm (624.568 THz) or 510 nm (587.828 THz) for ^{85}Rb or ^{133}Cs, respectively. When the atoms are exposed to the coupling lasers, they are excited to a higher atomic state, i.e. to a Rydberg state. An interference of the two atomic states occurs due to the presence of both the probe and coupling lasers. It induces transparency of the atoms to the probe laser. This effect is known as EIT, where a medium that is normally absorbing becomes transparent in the presence of an electromagnetic field (in this case the coupling laser). The resulting spectrum of this effect is shown in the top curve of Figure 11.3a. Note that the three curves in this figure lay on top each other, but have been arbitrarily shifted them along the vertical axis for ease of viewing. A clear peak in this top curve indicates transmission near $\Delta_p = 0$; it appears as a result of exposing the atoms to the coupling laser. The additional peak to the left of the main EIT peak is related to the atomic structure of the atoms. Many additional peaks may be present for some configurations (see [14] for details).

If the wavelength of the coupling laser is judiciously chosen in order to excite the atoms to a high enough Rydberg state, the RF source will be resonant with a transition to a nearby Rydberg state, i.e. an RF atomic transition. In other words, when the atoms are preconditioned with both the probe and coupling lasers, the next atomic transition can be accessed with an RF source. This RF source, when resonant with the RF atomic transition, causes the EIT transmission line to split in two. This splitting is known as AT splitting, and an example of the effect on the EIT spectral curve is given in the middle (black) curve of Figure 11.3a.

The EIT spectral signal and the AT splitting can at times be weak signatures on the Doppler background (the probe absorption line). To increase the signal-to-noise ratio (SNR) of the EIT, we often modulate the coupling laser amplitude with a 50% duty cycle, 30 kHz square wave and detect any resulting modulation of the probe transmission with a lock-in amplifier. This removes the Doppler background and isolates the EIT signal. The black, dashed-line curve in Figure 11.3b shows a typical EIT signal from the lock-in amplifier. When the RF field is turned on, this EIT peak splits and the splitting frequency is indicated by Δf_m.

Frequency splitting of the laser transmission spectrum through the alkali atoms is easily measured and is directly proportional to the applied RF E-field amplitude. The optical frequency difference between the two new peaks, Δf_m, is directly related to the RF E-field strength through the following expression [10, 11]

$$|E| = 2\pi \frac{\hbar}{\wp} \frac{\lambda_p}{\lambda_c} \Delta f_m = 2\pi \frac{\hbar}{\wp} \Delta f_o \tag{11.1}$$

where $\hbar$ is Planck's constant, $\wp$ is the atomic dipole moment of the RF atomic transition (see the following), $\Delta f_o = \frac{\lambda_p}{\lambda_c} \Delta f_m$, and λ_p and λ_c are the wavelengths of the probe and coupling laser, respectively. The λ_p/λ_c ratio is needed to account for the Doppler mismatch of the probe and coupling lasers [19]. The coupling laser can also be scanned as opposed to the probe laser. In this case, the wavelength ratio in Eq. (11.1) is set to 1.0 (see Eq. (1) in [28]).

Changes in the power or strength of the RF E-field result in linear changes in the measured splitting frequency difference Δf_m. Thus, it is only necessary to know the dipole moment of the RF atomic transition, $\wp$, and the wavelengths of the two optical fields along with the universal constant, Planck's constant (which is known by definition [5–7]) in order to obtain the E-field strength of the RF field at the atoms. It should be emphasized that this simple measurement only detects the magnitude of the RF E-field. Section 11.5 will discuss extensions to the measurement scheme that allow for detection of the RF E-field phase in addition to the magnitude. Because the atoms only respond to the RF field where the probe and coupling lasers overlap, the spatial resolution of this

field measurement can be quite small. This feature opens up the opportunity to perform imaging (even sub-wavelength imaging [14, 46]) or beam profiling measurements with arrays of such atom probes. These applications will also be discussed in Section 11.8.

This RF field measurement with the Rydberg atoms is a direct, SI-traceable measurement where the only unknown is the dipole moment, $\wp$, which can be calculated accurately to 0.1% [11, 22, 47]. Figure 11.4 shows the results of such a calculation for a particular RF atomic transition for both rubidium (^{85}Rb) and cesium (^{133}Cs) atoms. From these results we see that ^{85}Rb and ^{133}Cs have similar values for the radial dipole moment $\mathcal{R}_{RF}$ or the normalized dipole moment Q_{RF}, i.e. $\mathcal{R}_{RF}/a_0$, where $a_0 = 0.529\,177 \times 10^{-10}$ m is the Bohr radius. These large values of $\mathcal{R}_{RF}$ for these Rydberg states is what makes this technique beneficial for measuring RF E-fields. While either of these two atoms can be used, ^{85}Rb nevertheless has some advantages when performing measurements at the high RF end of the spectrum. On the other hand, ^{133}Cs has some advantages at the low RF end of the spectrum. The other advantage of ^{133}Cs that may be useful in some situations is that ^{133}Cs has a higher vapor pressure than ^{85}Rb [48, 49]. Both ^{133}Cs and ^{85}Rb were used in the various experiments presented in this chapter.

Figure 11.5 shows a comparison of measurements of the E-field strength with the Rydberg atom sensor to results obtained from calculations based on Maxwell's equations (based on Eq. (3) in [38]). These results illustrate the validity of the Rydberg atom-based technique. They also illustrate that a single probe has the ability to measure fields ranging from hundreds of megahertz to the lower terahertz spectrum.

The broadband nature of this technique is due to the large number of possible Rydberg states that can exhibit a large response to an RF source. These states form a discrete set of frequencies that can be measured. The RF source must be tuned to the precise frequency (within a given bandwidth) that corresponds to an atomic transition. The wavelength of the coupling laser selects the transition that will respond to the RF source, which defines the frequency that will be measured. While there are a large number of possible atomic states with RF transition frequencies, several of these have

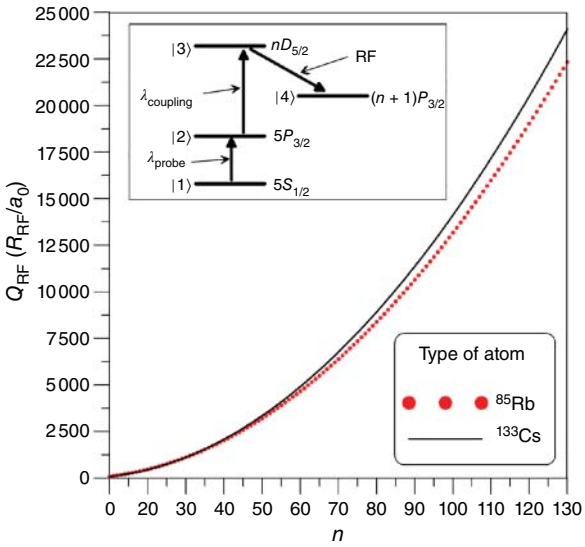

Figure 11.4 Calculations of Q_{RF} ($\mathcal{R}_{RF}/a_0$) for a particular RF atomic transition for ^{85}Rb and ^{133}Cs. The inset shows the atomic levels for ^{85}Rb and ^{133}Cs, where n is the principal quantum number and "D" and "P" indicate the angular momentum state of the atoms. Source: From [12] / with permission from IEEE.

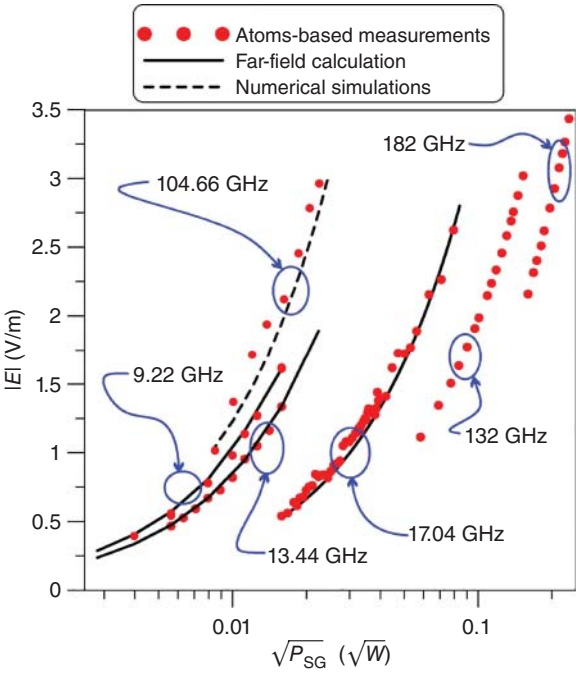

Figure 11.5 Comparison of the results obtained with Rydberg atom-based techniques to those calculated with Maxwell's equations. Source: From [50] / with permission from IEEE.

small atomic dipole moments. Since the measurement splitting (Δf_m) is directly proportional to the atomic dipole moment, as shown in Eq. (11.1), we want to use RF transitions with large dipole moments. One typically uses the four RF transitions corresponding to $nD_{5/2} - (n+1)P_{3/2}$, $nD_{5/2} - (n-1)F_{5/2}$, $nS_{1/2} - nP_{3/2}$, and $nS_{1/2} - (n-1)P_{3/2}$, where "S," "P," "D," and "F" indicate the angular momentum state of the atoms [51].

We note that a scheme has recently been developed that allows for continuous frequency detection of weak RF fields [52]. This technique allows for the detection of an RF field signal over a frequency range that covers from one Rydberg state with principal quantum number n to the next $n+1$ state. Such an approach allows for the development of a spectrum analyzer and waveform detector. Continuous frequency detection of strong field strengths can also be done with Stark shifts approaches [53].

While the on-resonant EIT/AT scheme discussion earlier has been very successful in detecting field levels in the range of 5 μV/m [10–12, 33, 34] to tens of V/m, the EIT/AT poses two problems. First, once the field strength becomes too large, AT peaks become difficult to resolve (e.g. see the +6 dBm case in Figure 18 in [11]). Secondly, the EIT/AT scheme requires the RF signal of interest to be resonant with the Rydberg transition as the scheme only detects frequencies within the narrow bandwidth of a Rydberg transition. For strong and off-resonance fields, AC Stark shifts [16–18] or, more generally, a Floquet method [18] are used. A strong RF field – either on or off resonance – can cause the EIT signal to shift in frequency, e.g. see Figure 11.6. The shift is related to the square of the magnitude of the applied RF field [54] and, hence, provides a means to detect strong field strengths.

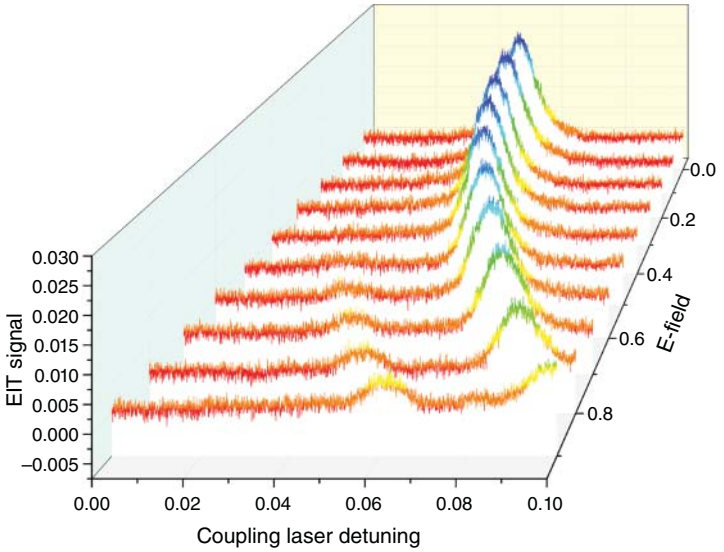

Figure 11.6 AC Stark shift due to a high intensity RF field.

11.3 Uncertainties

As introduced earlier, this method for RF E-field measurement provides a potential for absolute, SI-traceable calibrations. In order for these measurements to serve SI-traceable calibrations, it is important to understand the sources of uncertainty. Initial investigation into the uncertainty contributions have been done in [10, 20], and [55]. These studies found the most significant sources of uncertainty to be laser intensity noise, electrical detection noise, and the effect of the vapor cell on the microwave field. Laser and electronic noise can be minimized through various schemes. The vapor cell, typically constructed from dielectric glass, has a relatively low permittivity in the microwave range. However, the cell can still cause standing waves to arise inside where the atoms are probed. This causes a difference between the field seen by the atoms and the field outside the vapor cell, dependent on the microwave frequency, geometry of the vapor cell, and the location of the measurement inside the cell [56]. This discrepancy can be large. This can be calibrated out by measuring the whole standing wave pattern inside the cell [14, 55, 56].

While the cell can perturb the E-field measurement, vapor cell designs can be pursued to minimize and even eliminate the vapor cell perturbations. Various groups are investigating different approaches to modify the vapor cell used for these Rydberg atom-based sensors. Two examples include the use of vapor cells with honeycomb sides [57] or the use of metamaterials on the sides of the vapor cells [58].

11.4 Detection of AM and FM Modulated Signals

The Rydberg EIT system can respond to time-varying RF signals. This includes both amplitude modulated (AM) and frequency modulated (FM) signals. Modulating either the amplitude or frequency of a resonant RF field (or "carrier") causes the AT peak separation to vary in time (see [28]

for details). The Rabi frequency is defined as:

$$\Omega = \frac{\wp}{\hbar} |E| \tag{11.2}$$

If the modulation amplitude effective Rabi frequency is large compared with the EIT or AT linewidth, the peak location in laser frequency detuning will vary proportionally to the modulation. If the modulation amplitude effective Rabi frequency is small compared with the EIT or AT linewidth, this AT peak shift appears as a variation in the probe transmission for fixed laser detunings.

For the case where the mean RF field amplitude Rabi frequency is less than the EIT linewidth, it is important to note the behavior of the EIT line. Below this threshold for AT splitting, the EIT line amplitude reduces with increased RF field amplitude. In this regime, an AM RF signal will cause a direct modulation of the EIT amplitude.

Figure 11.7a shows a simulation of the AT splitting for three different RF field amplitudes. By setting the laser detuning to zero, the probe transmission directly follows the amplitude modulation. Therefore, no demodulation circuitry is needed to retrieve the modulated signal from the carrier. The transmission value is highlighted by the circle for each case.

For higher field strengths, the AM can still be detected, as shown in Figure 11.7b. The transmission value at the laser frequency is again highlighted by the dots. In this case the laser must be detuned and locked near one of the AT peaks, which no longer is near $\Delta = 0$. As the field amplitude increases and decreases, the peak location shifts. This shift again causes the probe transmission to follow the baseband modulation.

Frequency modulation creates a very similar result [28] for relatively weak fields. The laser detunings can then be set to zero, and the probe transmission will directly follow the frequency modulation. For stronger fields, the lasers must again be detuned to find the shifted AT peak. The probe transmission will then continue to the follow the frequency modulation. This behavior is illustrated in Figure 11.7c. It effectively converts an RF FM signal into an optical AM signal directly, without demodulation electronics. More discussion on how the atoms actually perform the demodulation is given in [28].

Various groups have demonstrated AM/FM reception using Rydberg-atom sensors [26–31]. Figure 11.8 shows a comparison of an original waveform to the received waveform from an AM and a FM modulated signal. Figure 11.9 shows the results for a received digital AM waveform. In this figure, we also illustrate the effect of noise on the reception. Groups are currently investigating the effect of noise on these types of Rydberg atom-based receivers and sensors in order to understand if the atom-based systems have better noise rejection. For example, [25] investigates how white Gaussian noise effects these types of measurements, where it is shown that detection is possible even for very low SNRs.

11.5 Phase Detection and Phase Modulated Signal Detection

The Rydberg EIT signal is not directly sensitive to the phase of an RF field. The response rates that we have observed are limited to tens of MHz. They are sensitive to changes in the field amplitude due to constructive or destructive interference from the addition of other resonant RF fields. This sensitivity has been used to map out standing waves inside of the dielectric vapor cells [12, 14, 56], as well as inside of metallic waveguides (Section 11.6). In this section, we show how Rydberg EIT can detect the phase of an unknown RF signal by applying a second, well-characterized RF field of a similar frequency.

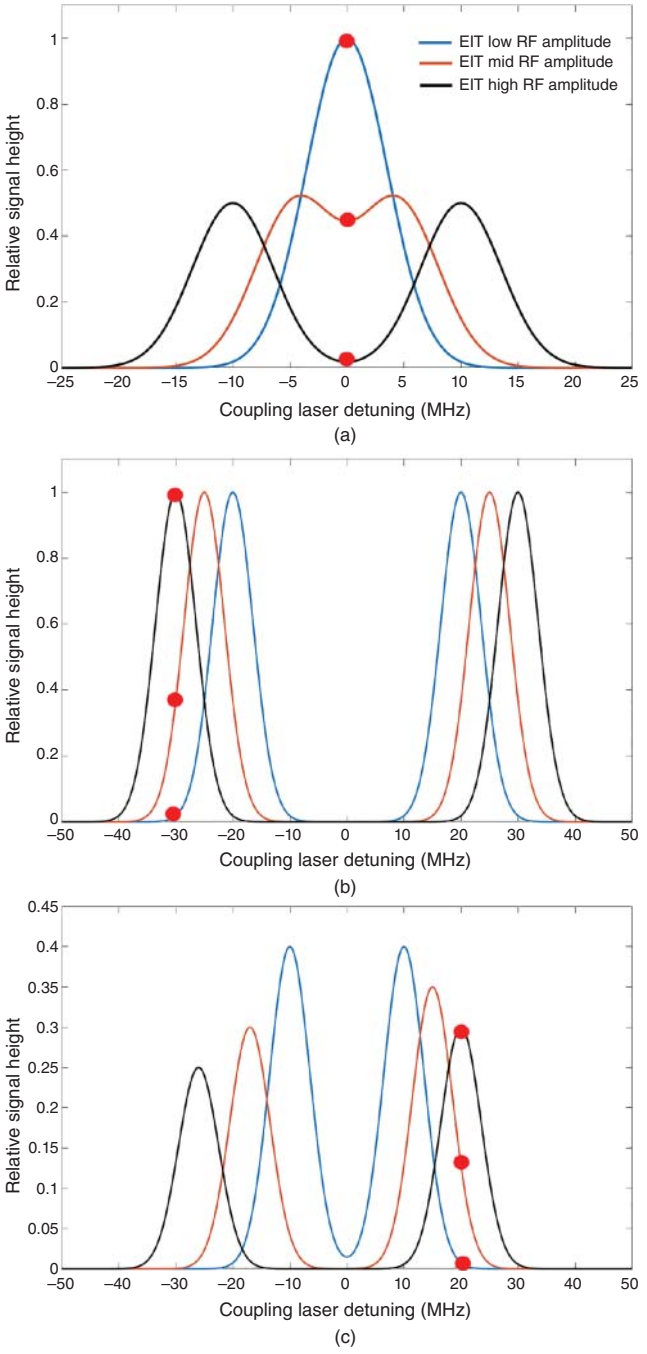

Figure 11.7 Simulations of AT spectra for different RF field amplitudes, demonstrating the effect of a modulated RF signal on the probe field transmission. The probe transmission is shown relative to a maximum EIT signal. The dot illustrates the probe transmission for fixed probe and coupling laser frequencies where there is significant modulation. Each trace is for a different RF field strength at different times within the modulation period. Three interesting cases are: (a) Amplitude Modulated RF signal for a relatively weak RF field, where maximum modulation is near zero laser detuning; (b) strong RF field carrier with an AM signal, where the lasers are detuned to an AT peak; (c) a Frequency Modulated RF signal, where the detection results in an amplitude modulated probe transmission.

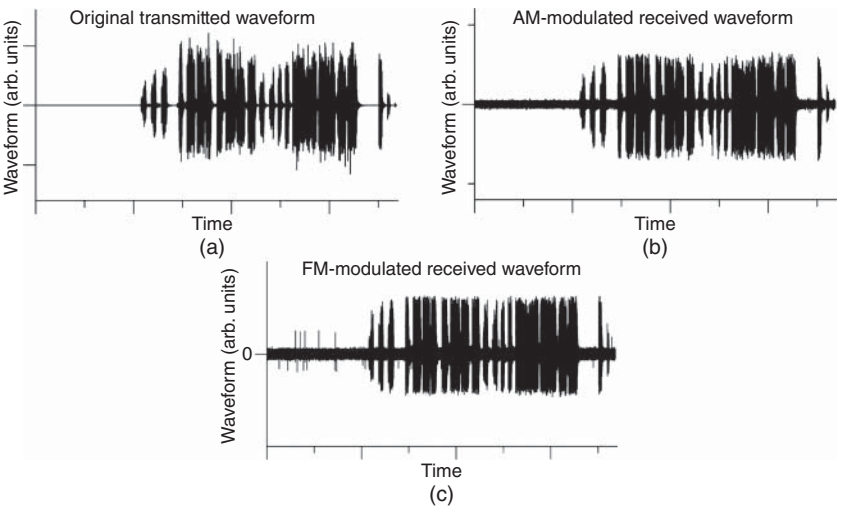

Figure 11.8 Waveforms associated with the atom-based stereo receiver when the signal is either amplitude or frequency modulated. (a) Transmitted waveform. (b) Received waveform from the AM modulation scheme. (c) Received waveform from the FM modulation scheme.

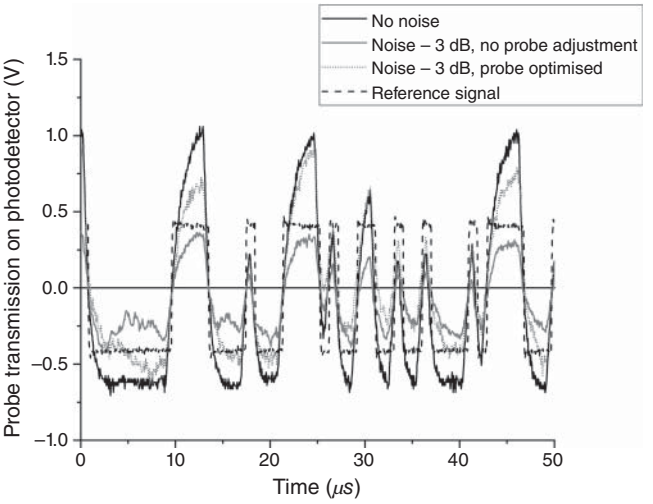

Figure 11.9 Examples of a digital AM waveform received by the atoms under different measurement conditions.

Details on how phase detection is achieved are given in [32, 39]. A single RF field near resonance, denoted as local oscillator or LO field, will cause a Rydberg peak to reduce in amplitude. It will then undergo AT splitting (as discussed in Section 11.2) as the LO field strength is increased. Fixing the probe laser frequency to the center of the EIT signal, the output will appear as a decrease from a maximum value (with zero LO field strength) to zero (corresponding to an LO field strength where the AT peaks are well-separated and beyond). Consider the case where the LO field strength is fixed such that the EIT signal is midway between its maximum and minimum values. Any constructive or destructive interference from another source will cause the total field strength to change, and thus cause the EIT signal to rise or fall. If a second RF signal (defined as

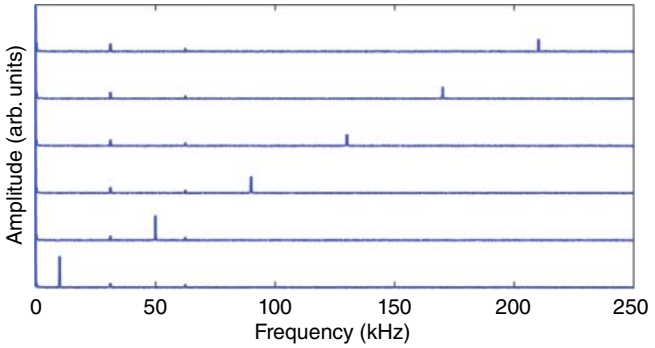

Figure 11.10 Example of the transmitted probe spectrum for various difference frequencies between the SIG and LO fields.

SIG) field is applied with the same frequency as the LO, the two field strengths sum according to their phase difference. In the case where the amplitudes are equal, the EIT signal will reduce to zero if they are in phase. On the other hand, if they are perfectly out of phase, the EIT signal increases to its maximum value as if there was no RF field present. This results in a phase sensitive homodyne detection of the RF SIG field [32, 39].

If a SIG field is applied that is detuned in frequency from the LO, the EIT signal will oscillate in time at the difference frequency (or intermediate frequency [IF]) between the SIG and LO. In this atom mixer or superheterodyne configuration, the phase of the IF signal is directly related to the difference between the SIG and LO phases. Figure 11.10 shows examples of the spectrum of the transmitted probe laser for various IF (Δf) frequencies. The power spectrum of the transmitted probe field shows the IF signals present; their amplitudes can then be directly related to the SIG field strength [32, 34].

The heterodyne technique allows for a much more sensitive detection of the RF signals. The AT splitting method is limited to measuring RF field amplitudes equivalent to Rabi frequencies close to the EIT linewidth [20], and the EIT amplitude-only approach is limited to 80 μV/m [10]. In contrast, the atom mixer approach can provide sensitivities down to 55–700 nV/cm$\sqrt{\text{Hz}}$ [33, 34]. As a low-frequency signal is created in the presence of the RF signal of interest, this signal can be detected through lock-in amplification of the photodetector signal. This allows for sub-Hz frequency selection [33]. Heterodyne reception can also be observed through the AC Stark effect with higher RF field strengths. Such a configuration was used to create an atom-based spectrum analyzer from DC - 20 GHz [35].

With phase-sensitive detection, the Rydberg atom sensor can now be used to receive traditional phase modulated (PM) signals. While AM and FM have been used for simple analog transmission, most digital communications schemes rely on phase modulation. Typical schemes include binary phase-shift keying (BPSK), quadrature phase-shift keying (QPSK), and quadrature and amplitude modulation (QAM). Rydberg atoms have been used to down-convert the carrier to the baseband modulation for these types of signals, where the resulting photodetector signal was sent to a vector signal analyzer for demodulation [30]. Figure 11.11 shows the IQ-diagram for QPSK and 16-QAM received signals obtained from the Rydberg atom-based receiver [30]. The atom-based mixer has also been used to measure the propagation constant of free space [32, 39] and for measuring the phase of a microwave device [39, 59].

While applying a second RF field (the LO) to create an atom-based mixer has been shown to be successful, this approach does have some disadvantages. Foremost is the need to apply a second

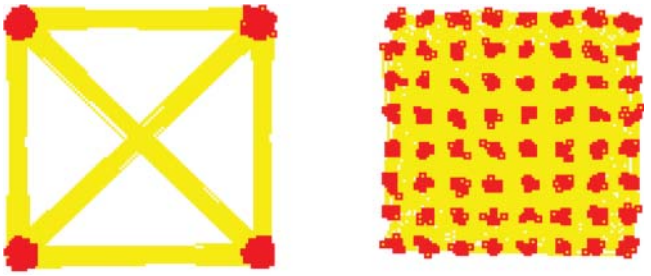

Figure 11.11 Example of the IQ-diagram from received phase-modulation signals: (a) QPSK, and (b) 64-QAM. Source: From [30] / with permission from IEEE.

RF field. To overcome this, an all-optical phase detection approach is desired. Various all-optical approaches are currently being investigated and one approach is given in [60].

11.6 RF Power Measurements

In addition to RF E-field strength measurements, RF power measurements and calibrations are very important in all electromagnetic systems, including radar and advanced communications applications. A Rydberg atom-based sensor placed in rectangular waveguide can be used for this purpose [23], see Figure 11.12. The power carried by the fundamental mode of a rectangular wave guide is given by

$$P = E_o^2 \ \frac{ab}{4} \sqrt{\frac{\epsilon_o}{\mu_o}} \ \sqrt{1 - \left(\frac{c}{2af}\right)^2} \tag{11.3}$$

where E_o is the amplitude of the E-field at the center of the waveguide and a and b are the cross-sectional dimensions of the rectangular waveguide where a is the larger dimension as indicated in the inset in Figure 11.12. The frequency is f; ϵ_o and μ_o are the permittivity and

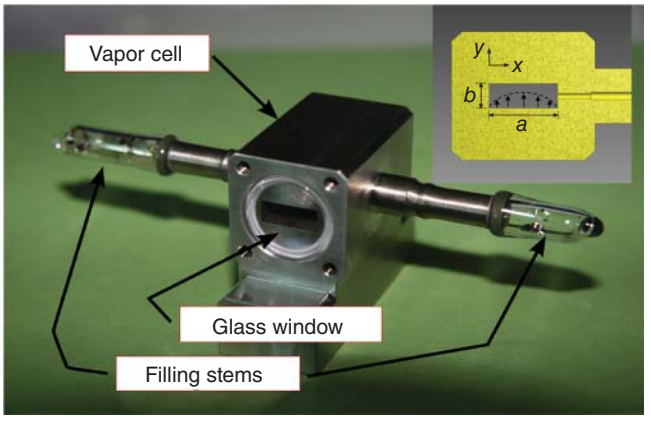

Figure 11.12 WR-42 rectangular waveguide vapor cell with waveguide dimensions. The vapor cell consists of a 34-mm section of waveguide with glass windows attached to each end that is filled with the atomic vapor. Source: From [23] / with permission from AIP Publishing LLC.

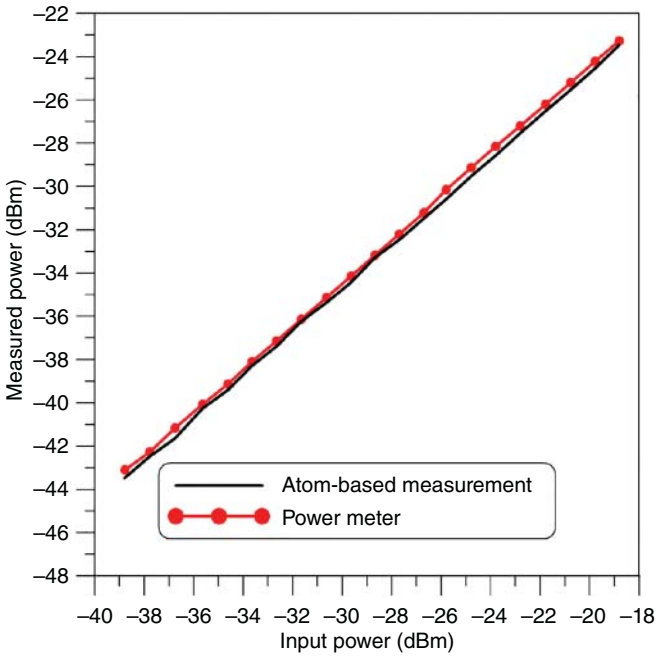

Figure 11.13 Measurements of the power in the waveguide versus the input power at 19.629 GHz. Source: From [23] / with permission from AIP Publishing LLC.

permeability of free space; and c is the speed of light in *vacuo*. As discussed in [23], the Rydberg atoms are used to measure E_o for a given input power. The power propagating through the waveguide is determined with Eq. (11.3).

Figure 11.13 shows a comparison of the power measured with the Rydberg atom-based approach to that obtained with a conventional power meter. The comparison shows very good correlation between the two methods. When compared with conventional power metrology approaches, the Rydberg atom-based approach: (i) is a more direct SI-traceable approach, (ii) has the possibility of having much lower uncertainty, (iii) exhibits a large frequency range, and (iv) has much better dynamic range (i.e. power-level ranges). Furthermore, the Rydberg atom-based approach can lead to "real-time" in situ calibrated sources.

11.7 Voltage Measurements

EIT and Stark shifts in Rydberg atoms can be used for the measurement of direct current (dc) and 60 Hz alternating current (ac) voltages [40]. This section describes the atom-based measurements of the dc and ac voltages with an emphasis on how they may lead to the potential calibration of voltage instrumentation. A Rydberg atom-based dc (or 60 Hz) voltage measurement is performed by observing the dc (quasi-dc) differential Stark shift in the Rydberg states, which is given by the expression [54]:

$$\Delta = \frac{\alpha}{2} \; E^2 \tag{11.4}$$

where Δ is the Stark shift (in units of Hz), E is the applied E-field (in units of V/m) at the frequency f (in units of Hz), and α is the polarizability of the atom (in units of Hz/(V^2/m^2)).

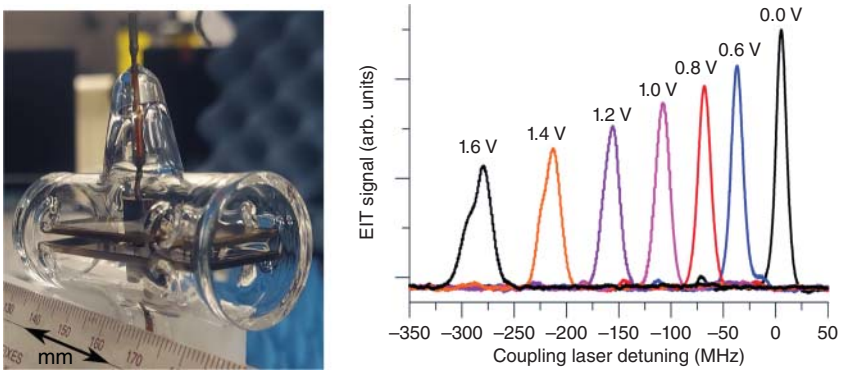

Figure 11.14 Rydberg-atom based voltage measurement. (a) Cylindrical vapor cell with stainless-steal parallel plates. The vapor cell is 50 mm in length and has an outside diameter of 25 mm. The plates are rectangular in shape with width of 18 mm, length of 45 mm, and separation of ≈ 2mm. (b) dc Stark shift due to an applied voltage across the parallel plates in the cell shown in (a). Source: (a) From [40] / arXivLabs / CC BY 4.0.

We measure the voltage induced between two parallel plates embedded in an atomic vapor cell as shown in Figure 11.14a by measuring the Stark shifts in the atomic spectra of the Rydberg atoms. If a voltage is applied across two parallel plates separated by the distance d, then the E-field between the plates is $E = V/d$. By substituting this result into Eq. (11.4), the voltage can be found by a measurement of the Stark shift as:

$$V = d\sqrt{\frac{2\,\Delta}{\alpha}} \tag{11.5}$$

Figure 11.14b illustrates the Stark shift of the EIT signal as a function of an applied voltage. By measuring the Δ and using Eq. (11.5), the applied voltage can be determined. These types of Rydberg atom-based voltage measurements are currently being investigated as an alternative for Josephson-junction based standards and Zener-diode voltage references [40].

11.8 Other Applications: RF Camera, Angle-of-Arrival, Waveform Analyzer, Plasma Measurements, and Thermometry

The atom-probe systems that we have described up to this point have been bound to an optical table due to the alignment requirements of the two (or many) lasers within the atomic vapor cell. Such constraints, though, are not absolute. The optical fields needed for the atom RF probe measurements can be transferred to the vapor cell through well-aligned optical fibers. Even the returning probe laser, which carries the susceptibility information linked to the RF field, is passed back through the optical fibers. This separates the laser generation and detection from the vapor cell where the measurement occurs, creating a movable RF probe head consists of only the dielectric vapor cell with bonded optical fibers. A photograph of such a sensor head is given in Figure 11.15.

Fiber connections afford greater mobility. Hence, they expand the range of E-field measurements and calibrations that can be completed with the atom probes because a probe can be brought to the RF source or into an environment of interest. In addition, the all-dielectric probe head is especially valuable as it minimally scatters the RF field(s). Traditional, metallic probes and antennas have a

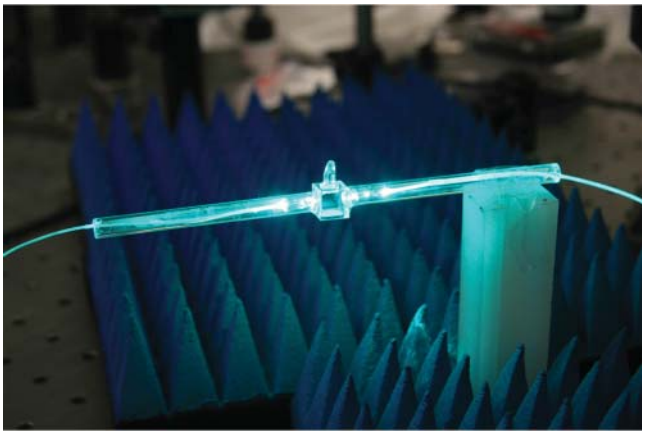

Figure 11.15 Photograph of a fiber-coupled atom probe. Source: From [12] / with permission from IEEE.

relatively large coefficient of reflection. A significant fraction of the incident RF field will scatter off the probe and may return, after subsequent scattering events, back to the probe. Such scattering off the probe is problematic for accurate measurements of phase, AoA, and channel sounding measurements. The all-dielectric fiber-coupled (FC) atom probe, on the other hand, has a significantly lower coefficient of reflection at radio frequencies and offers an attractive alternative to traditional metallic probes, in addition to the SI-traceability and absolute accuracy benefits discussed in Section 11.2 of this chapter.

With the movable, all-dielectric FC atom probe, researchers can measure spatial variations of a static RF field by translating the probe or moving a horn antenna with respect to the probe. For example, a horn gain pattern was measured [24], showing the spatial distribution of the power emitted by the horn. The measurements confirmed that the fiber probe resolves differences in the side lobe level of the antenna pattern between the H plane and E plane of propagation from the horn and showed good agreement with measurements made with a traditional device. Furthering the demonstration, the authors traced out the field pattern above a co-planar waveguide and in a transverse electromagnetic (TEM) test cell [50]. Measuring across the waveguide axis, they showed an M-shaped field distribution in the E-field strength that decays as the probe is moved away from the co-planar waveguide.

By placing the FC probe on a translation stage, it is possible to map out the relative change in magnitude and phase of an RF signal using the superheterodyne method described in Section 11.5. For example, horns for both the SIG (19.626 GHz) and LO RF fields are placed inside an anechoic chamber with the FC probe and a two dimensional (2D) translation stage. A system diagram is given in Figure 11.16a. At each (X, Y) position of the stage, a new beat note at the IF of 1 kHz is collected and the magnitude and relative phase of that beat note is extracted. The 2D maps of the magnitude and phase in Figure 11.16b,c give the relative change in each measurement either over the spatial area with respect to the measurement at ($X = 0$ mm, $Y = 0$ mm) or on-axis with the SIG horn.

This type of spatial acquisition of the RF field magnitude and phase through scanning can be used for channel sounding measurements. Channel sounding is a technique of evaluating the RF environment that a wireless signal interacts with between a transmitter and a receiver. Due to obstacles and scatterers in the environment, the wireless signal can follow multiple propagation paths. To optimize the signal at the receiver, engineers can use beamforming techniques and adaptive networks that overcome environmental losses experienced by the wireless

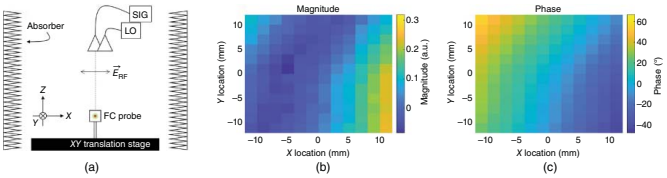

Figure 11.16 All-dielectric fiber-coupled (FC) Rydberg atom probe is placed inside an anechoic chamber with the RF signal (SIG, 19.626 GHz) and local oscillator (LO, 19.626 GHz + 1 kHz) horns. (a) Translating the probe in the *XY* plane results in measured spatial distributions of the (b) relative RF field magnitude and (c) phase.

signal. However, a well-characterized environment, or channel, is required to design such signal improvement techniques. The all-dielectric, FC atom probe with its minimized perturbations to the RF fields can be used to measure and characterize such a channel. We can demonstrate this by returning to the anechoic chamber example in Figure 11.16, but this time with a scatterer placed in the $+X$ direction to modify the relative magnitude and phase measurements. Differences between the measurements without the scatterer and with the scatter, shown in Figure 11.17, confirm that the probe does resolve the subtle changes to the RF field in the plane of the translation stage when the scatterer is added to the environment.

One drawback of the single-point FC probe, like that photographed in Figure 11.15, is that the probe must be translated in order to obtain spatially variant information from a scene. This means that the RF fields cannot change over the time it takes to complete a full 2D scan. An alternative to this technique is to build an atom-based sensor that consists of an array of probes.

The active area of the Rydberg atom probe is defined by the overlapping region of the probe and coupling lasers. This small, well defined area of the RF field sensitivity can, therefore, be leveraged to build RF field cameras. The design of such a camera is a simple extension to the FC probe discussed earlier. Within the vapor cell, the propagation paths of the two lasers are defined in such a manner that the vapor cell area is segmented into pixels. Each pixel is then addressed by either modulating or switching the lasers in each row and column. Optical fibers are again used to transfer the laser fields to the vapor cell. A photonic integrated circuit may be used to streamline the transfer of the laser fields to each pixel within a compact overall package. To date, such an RF field camera has yet to be demonstrated. Nevertheless, our group is currently developing such architectures for an RF camera and RF beam profiler. Rydberg atom probe arrays of this kind will have many benefits over the single-point probes currently in development. For one, acquisition of 2D field information can be captured within the time needed to read out each pixel of the array. If each pixel has its own detector for reading the transmitted probe power, then the read out time could be as fast as the integration time needed to obtain an acceptable SNR at a single pixel. RF E-field beam profiling and fast acquisition of channel sounding measurements would be possible with these arrays. Furthermore, the entire array can be constructed from purely dielectric materials. This removes the translation stage from the acquisition process, which can otherwise contribute to undesirable scattering of the RF field.

The ability to measure AoA is of great importance to radar and advanced communications applications. Measuring the phase of an RF field in different locations in space affords a determination AoA of an incident RF field. Recent work has shown that this can be accomplished by determining the phase of an incident RF field in various locations inside an atomic vapor cell [36]. Figure 11.18 shows a comparison of the measured AoA of an incident RF field to the actual incidence angle. These results show that compact atom-based sensors can be used for determining the AoA. One can envision (i) developing arrays of these Rydberg atom sensors or (ii) sampling the phase at numerous locations inside one vapor cell in order to detect the AoA from more general incidence angles. This measurement may also be used for the purpose of simultaneously detecting the AoA of several sources at once. Other work has shown that by sampling the phase of an incident RF field at various locations in a vapor cell, one can characterize other aspects of an RF source and increase its data capacity [61].

The phase measurement of an RF signal also allows for waveform analysis and even a Rydberg atom-based spectrum analyzer [35, 62]. As an example, Figure 11.19 shows the received waveform obtained with a Rydberg atom-based sensor in response to an incident chirp signal. The frequency of the RF source was linearly increased to generate the chirp. The atoms in the heterodyne mixer

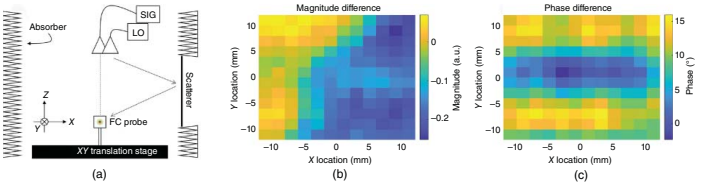

Figure 11.17 The setup (a) is the same as in Figure 11.16, but now a scatterer located in the $+X$ direction is added to the chamber resulting in measurable differences in the measured E-field (b) magnitude and (c) phase.

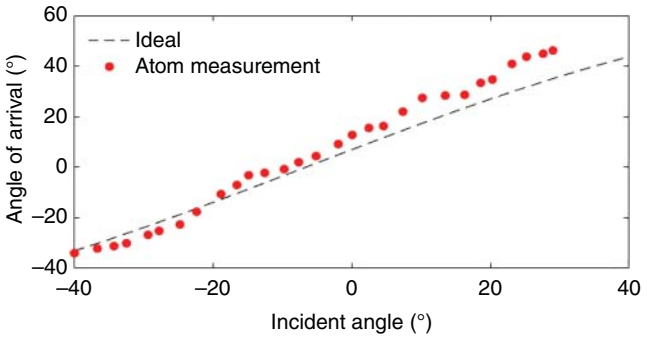

Figure 11.18 An RF SIG horn is rotated with respect to an LO horn such that the angle of incidence of the SIG RF field on a Rydberg atom vapor cell is changed. The difference in the phase measured by two optical probes within the vapor cell is used to determine a measured value of the angle-of-arrival (AoA) of the SIG RF field. These data demonstrate the ability to measure the AoA. Nonetheless, some refinement of the technique is required to improve its accuracy.

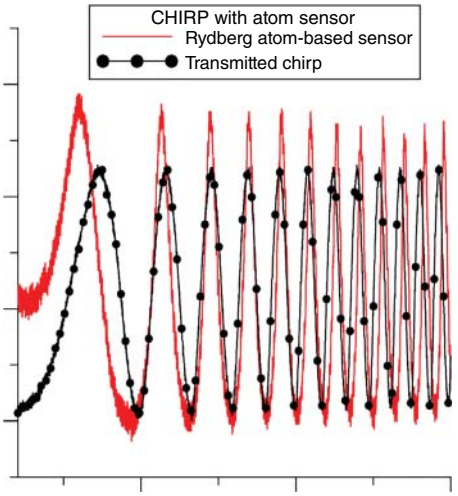

Figure 11.19 Received chirp signal.

configuration show the deviation of the RF source from the frequency of the applied LO by registering the beat note between the two. The atom signal obtained in this manner is compared with a classical mixer between the LO and RF source.

In addition to the aforementioned discussed applications, Rydberg atom sensors have been shown to be useful as a non-invasive method of measuring and characterising plasmas [63] and for possible blackbody thermometry [64]. In fact, current work is being performed to investigate the possibility of using Rydberg atom-based sensors for the detection of blackbody radiation (BBR). If successful, this could lead to a new SI-traceable method of calibrating BBR sources and instrumentation.

11.9 Conclusion and Discussion

Rydberg atoms show much promise as a paradigm shift in electromagnetic sensors wherein sensor elements are no longer realized through lumped circuit elements or semiconductor devices,

but rather as a naturally occurring and fundamental physical system: the atom. As has been summarized in Sections 11.4 and 11.5, Rydberg atoms have the ability to act as atomic sensors and receivers in a variety of modalities. Thus far, they have been demonstrated for measuring a number of electromagnetic quantities including field amplitude and phase, modulated signals, power, and voltage. Fundamental aspects of Rydberg atoms should be pointed out for which future applications and discoveries will undoubtedly leverage the use of Rydberg atoms.

The ability of a Rydberg atom to act as a transducer between the RF amplitude and optical frequency via the Rabi frequency is at the core of many of the sensor applications. Through this property, the atoms are able to link two vastly differing size scales – some nine orders of magnitude – between the optical domain ($\lambda \approx 10^{-9}$ m) and the RF domain ($\lambda \approx 1$ m). This feature facilitates a unique and advantageous scenario wherein the Rydberg atoms are able to resonantly operate and detect electromagnetic fields well below the cutoff wavelength of RF systems. Applied in creative ways, one can realize new measurement opportunities. For instance, as discussed in Sections 11.1 and 11.6, the probe can act as an electrically small RF antenna or be applied to waveguide power measurements, respectively.

Another consequence of the transduction property between the RF and optical domains is that the required optical tuning range to access the atomic transitions provided by the Rydberg atoms for sensing applications are easily attainable by available laser systems. As such, a single laser system can now replace a whole host of RF equipment that would be needed in order to span the operating range of Rydberg atom species, e.g. from hundreds of MHz to 1 THz with Cs and Rb. This reduction in equipment requirements adds to the possibility for compact Rydberg atoms based sensors and arrays of sensors. Integration with other atomic devices, such as atomic clocks, also becomes possible as the laser systems are common for alkali atoms in general.

Being a natural system, Rydberg atoms provide a fundamental standard measurement of electromagnetic quantities. Another consequence of the transduction property via the Rabi Frequency is that measurements with Rydberg atoms become traceable to the SI via Planck's constant. This traceability is advantageous as oftentimes its path in more conventional electromagnetic measurements relies heavily on measuring the shape and/or position of an antenna within an anechoic environment. This can become time consuming and can result in a chicken-and-egg traceability path dilemma. The body of work related Rydberg atoms studies is not new per se, but the comparatively recent increased interest and advances in the application of Rydberg atoms as electromagnetic sensors points to an exciting future of new ideas and metrology methods using the ever so humble atom.

The techniques discussed in this chapter allow for the development of an E-field probe that does not require a calibration because an absolute value of the field is determined by the atomic properties of the Rydberg atom itself. Moreover, they provide self-calibrating, direct SI-traceable methods for RF E-field metrology. Furthermore, we have also discussed the ability to measure RF power. As a consequence, a Rydberg probe can lead to a direct SI-traceable approach for power metrology. The relationships and measurement demonstrations discussed herein are the first step toward the realization of quantum-based RF power and RF E-field strength measurement techniques and toward the realization of a more direct link to the newly redefined SI. Other applications include: waveform and spectrum analyzers, AoA sensors, voltage measurements, RF cameras and sensor arrays, and receivers for communication signals (AM/FM modulated and digital phase modulation signals). In the past ten years of the development of the Rydberg atom-based sensors, we have learned to control ensembles of room-temperature atoms in such a manner that we are able to develop interesting and unique applications. As a result, unforeseen applications are emerging each day.

References

1 J. S. Belrose, "Reginald Aubrey Fessenden and the birth of wireless telephony," *IEEE Antenna Propag. Mag.*, vol. 44, no. 2, pp. 33–47, 2002.

2 G. Pelosi, "Foreword from the associate editor," *IEEE Antenna Propag. Mag.*, vol. 54, no. 4, p. 283, 2012.

3 J. S. Belrose, "A Fessenden Christmas Eve broadcast retrospective," *IEEE Antenna Propag. Mag.*, vol. 54, no. 4, pp. 285–287, 2012.

4 M. Born, *Einstein's Theory of Relativity*. New York: Dover Publications, Inc., 1965.

5 NIST. Metric-Program. Si units. https://www.nist.gov/pml/weights-and-measures/metric-si/si-units, June 2021.

6 D. B. Newell, F. Cabiati, J. Fischer, S. G. Fujii, K. Karshenboim, H. S. Margolis, E. de Mirandés, P. J. Mohr, F. Nez, K. Pachucki, T. J. Quinn, B. N. Taylor, M. Wang, B. M. Wood, and Z. Zhang, "The CODATA 2017 values of h, e, k, and n_a for the revision of the SI," *Metrologia*, vol. 55, no. 1, pp. 13–16, 2018.

7 M. Stock, "The revision of the SI towards an international system of units based on defining constants," *Meas. Tech.*, vol. 60, no. 12, pp. 1169–1177, 2018.

8 T. F. Gallagher, *Rydberg Atoms*. Cambridge: Cambridge University Press, 1994.

9 J. A. Gordon, C. L. Holloway, S. Jefferts, and T. Heavner, "Quantum-based SI traceable electric-field probe," in *2010 IEEE International Symposium on Electromagnetic Compatibility, July 25–30*, pp. 321–324, 2010.

10 J. A. Sedlacek, A. Schwettmann, H. Kubler, R. Low, T. Pfau, and J. P. Shaffer, "Microwave electrometry with Rydberg atoms in a vapour cell using bright atomic resonances," *Nat. Phys.*, vol. 8, no. 11, pp. 816–824, 2012.

11 C. L. Holloway, J. A. Gordon, A. Schwarzkopf, D. A. Anderson, S. A. Miller, N. Thaicharoen, and G. Raithel, "Broadband Rydberg atom-based electric-field probe for SI-traceable, self-calibrated measurements," *IEEE Trans. Antenna Propag.*, vol. 62, no. 12, pp. 6169–6182, 2014.

12 C. L. Holloway, M. T. Simons, J. A. Gordon, P. F. Wilson, C. M. Cooke, D. A. Anderson, and G. Raithel, "Atom-based RF electric field metrology: From self-calibrated measurements to subwavelength and near-field imaging," *IEEE Trans. Electromagn. Compat.*, vol. 59, no. 2, pp. 717–728, 2017.

13 M. Tanasittikosol, J. D. Pritchard, D. Maxwell, A. Gauguet, K. J. Weatherill, R. M. Potvliege, and C. S. Adams, "Microwave dressing of Rydberg dark states," *J. Phys. B*, vol. 44, 184020, 2011.

14 C. L. Holloway, J. A. Gordon, A. Schwarzkopf, D. A. Anderson, S. A. Miller, N. Thaicharoen, and G. Raithel, "Sub-wavelength imaging and field mapping via electromagnetically induced transparency and Autler–Townes splitting in Rydberg atoms," *Appl. Phys. Lett.*, vol. 104, 244102, 2014.

15 J. A. Gordon, C. L. Holloway, A. Schwarzkopf, D. A. Anderson, S. A. Miller, N. Thaicharoen, and G. Raithel, "Millimeter wave detection via Autler–Townes splitting in rubidium Rydberg atoms," *Appl. Phys. Lett.*, vol. 105, 024104, 2014.

16 D. A. Anderson, S. A. Miller, A. Schwarzkopf, C. L. Holloway, J. A. Gordon, N. Thaicharoen, and G. Raithel, "Two-photon microwave transitions and strong-field effects in a room-temperature Rydberg-atom gas," *Phys. Rev. A*, vol. 90, 043419, 2014.

17 D. A. Anderson, E. Paradis, G. Raithel, R. E. Sapiro, and C. L. Holloway, "High-resolution antenna near-field imaging and sub-THz measurements with a small atomic vapor-cell

sensing element," *2018 11th Global Symposium Millimeter Waves (GSMM), Boulder, CO*, doi: 10.1109/GSMM.2018.8439437, 2018.

18 D. A. Anderson, S. A. Miller, G. Raithel, J. A. Gordon, M. L. Bulter, and C. L. Holloway, "Optical measurements of strong microwave fields with Rydberg atoms in a vapor cell," *Phys. Rev. Appl.*, vol. 5, 034003, 2016.

19 A. K. Mohapatra, T. R. Jackson, and C. S. Adams, "Coherent optical detection of highly excited Rydberg states using electromagnetically induced transparency," *Phys. Rev. Lett.*, vol. 98, 113003, 2007.

20 C. L. Holloway, M. T. Simons, J. A. Gordon, A. Dienstfrey, D. A. Anderson, and G. Raithel, "Electric field metrology for SI traceability: Systematic measurement uncertainties in electromagnetically induced transparency in atomic vapor," *J. Appl. Phys.*, vol. 121, no. 23, 233106, 2017.

21 M. T. Simons, J. A. Gordon, C. L. Holloway, D. A. Anderson, S. A. Miller, and G. Raithel, "Using frequency detuning to improve the sensitivity of electric field measurements via electromagnetically induced transparency and Autler–Townes splitting in Rydberg atoms," *Appl. Phys. Lett.*, vol. 108, 174101, 2016.

22 M. T. Simons, J. A. Gordon, and C. L. Holloway, "Simultaneous use of CS and RB Rydberg atoms for dipole moment assessment and RF electric field measurements via electromagnetically induced transparency," *J. Appl. Phys.*, vol. 120, no. 12, 123103, 2016.

23 C. L. Holloway, M. T. Simons, M. D. Kautz, A. H. Haddab, J. A. Gordon, and T. P. Crowley, "A quantum-based power standard: Using Rydberg atoms for a SI-traceable radio-frequency power measurement technique in rectangular waveguides," *Appl. Phys. Lett.*, vol. 113, 094101, 2018.

24 M. T. Simons, J. A. Gordon, and C. L. Holloway, "Fiber-coupled vapor cell for a portable Rydberg atom-based radio frequency electric field sensor," *Appl. Opt.*, vol. 57, no. 22, pp. 6456–6460, 2018.

25 M. T. Simons, M. D. Kautz, C. L. Holloway, D. A. Anderson, and G. Raithel, "Electromagnetically induced transparency (EIT) and Autler–Townes (AT) splitting in the presence of band-limited white Gaussian noise," *J. Appl. Phys.*, vol. 123, no. 20, 203105, 2018.

26 D. H. Meyer, K. C. Cox, F. K. Fatemi, and P. D. Kunz, "Digital communication with Rydberg atoms and amplitude-modulated microwave fields," *Appl. Phys. Lett.*, vol. 112, 211108, 2018.

27 K. C. Cox, D. H. Meyer, F. K. Fatemi, and P. D. Kunz, "Quantum-limited atomic receiver in the electrically small regime," *Phys. Rev. Lett.*, vol. 121, 110502, 2018.

28 C. L. Holloway, M. T. Simons, A. H. Haddab, J. A. Gordon, D. A. Anderson, and G. Raithel, "A multiple-band Rydberg atom-based receiver: AM/FM stereo reception," *IEEE Antenna Propag. Mag.*, vol. 63, no. 3, pp. 63–76, 2021.

29 D. A. Anderson, R. E. Sapiro, and G. Raithel, "An atomic receiver for AM and FM radio communication," *IEEE Trans. Antennas Propog.*, vol. 69, no. 5, pp. 2455–2462, 2021.

30 C. L. Holloway, M. T. Simons, A. H. Haddab, J. A. Gordon, and D. Novotny, "Detecting and receiving phase-modulated signals with a Rydberg atom-based receiver," *IEEE Antenna Wireless Propag. Lett.*, vol. 18, no. 9, pp. 1853–1857, 2019.

31 Z. Song, H. Liu, X. Liu, W. Zhang, H. Zou, J. Zhang, and J. Qu, "Rydberg-atom-based digital communication using a continuously tunable radio-frequency carrier," *Opt. Express*, vol. 27, no. 6, pp. 8848–8857, 2019.

32 M. T. Simons, A. H. Haddab, J. A. Gordon, and C. L. Holloway, "A Rydberg atom-based mixer: Measuring the phase of a radio frequency wave," *Appl. Phys. Lett.*, vol. 114, 114101, 2019.

33 J. A. Gordon, M. T. Simons, A. H. Haddab, and C. L. Holloway, "Weak electric-field detection with sub-1 Hz resolution at radio frequencies using a Rydberg atom-based mixer," *AIP Adv.*, vol. 9, no. 4, 045030, 2019.

34 M. Jing, Y. Hu, J. Ma, H. Zhang, L. Zhang, L. Xiao, and S. Jia, "Atomic superheterodyne receiver based on microwave-dressed Rydberg spectroscopy," *Nat. Phys.*, vol. 16, pp. 911–915, 2020.

35 D. H. Meyer, P. D. Kunz, and K. C. Cox, "Waveguide-coupled Rydberg spectrum analyzer from 0 to 20 GHz," *Phys. Rev. Appl.*, vol. 15, 014053, 2021.

36 A. K. Robinson, N. Prajapati, D. Senic, M. T. Simons, and C. L. Holloway, "Determining the angle-of-arrival of a radio-frequency source with a Rydberg atom-based sensor," *Appl. Phys. Lett.*, vol. 118, 114001, 2021.

37 C. L. Holloway, M. T. Simons, A. H. Haddab, C. J. Williams, and M. W. Holloway, "A "real-time" guitar recording using Rydberg atoms and electromagnetically induced transparency: Quantum physics meets music," *AIP Adv.*, vol. 9, no. 6, 065110, 2019.

38 A. K. Robinson, A. B. Artusio-Glimpse, M. T. Simons, and C. L. Holloway, "Atomic spectra in a six-level scheme for electromagnetically induced transparency and Autler–Townes splitting in Rydberg atoms," *Phys. Rev. A*, vol. 103, 023704, 2021.

39 M. T. Simons, A. H. Haddab, J. A. Gordon, D. Novotny, and C. L. Holloway, "Embedding a Rydberg atom-based sensor into an antenna for phase and amplitude detection of radio-frequency fields and modulated signals," *IEEE Access*, vol. 7, pp. 164975–164985, 2019.

40 C. L. Holloway, N. Prajapati, J. E. Kitching, J. A. Sherman, C. Teale, A. Rüfenacht, A. B. Artusio-Glimpse, M. T. Simons, A. K. Robinson, and E. B. Norrgard, "Electromagnetically induced transparency based Rydberg-atom sensor for quantum voltage measurements,"*arXiv:2110.02335, Oct 22*, 2021.

41 M. Fleischhauer, A. Imamoglu, and J. P. Marangos, "Electromagnetically induced transparency: Optics in coherent media," *Rev. Mod. Phys.*, vol. 77, pp. 633–673, 2005.

42 K. J. Boller, A. Imamolu, and S. E. Harris, "Observation of electromagnetically induced transparency," *Phys. Rev. Lett.*, vol. 66, no. 20, pp. 2593–2596, 1991.

43 S. Kumar, H. Fan, H. Kubler, J. Sheng, and J. P. Shaffer, "Atom-based sensing of weak radio frequency electric fields using homodyne readout," *Sci. Rep.*, vol. 7, 42981, 2017.

44 J. P. Shaffer and H. Kübler, "A read-out enhancement for microwave electric field sensing with Rydberg atoms," in *Quantum Technologies 2018*, vol. 10674, J. Stuhler, A. J. Shields, and M. J. Padgett, Ed. International Society for Optics and Photonics, SPIE, 2018, pp. 39–49. https://doi.org/10.1117/12.2309386.

45 H. M. Kwak, T. Jeong, Y.-S. Lee, and H. S. Moon, "Microwave-induced three-photon coherence of Rydberg atomic states," *Opt. Commun.*, vol. 380, pp. 168–173, 2016. ISSN 0030-4018. Doi: 10.1016/j.optcom.2016.06.004. https://www.sciencedirect.com/science/article/pii/S0030401816304989.

46 H. Q. Fan, S. Kumar, R. Daschner, H. Kübler, and J. P. Shaffer, "Subwavelength microwave electric-field imaging using Rydberg atoms inside atomic vapor cells," *Opt. Lett.*, vol. 39, no. 10, pp. 3030–3033, May 2014. Doi: 10.1364/OL.39.003030. http://ol.osa.org/abstract.cfm?URI=ol-39-10-3030.

47 I. I. Sobelman, *Atomic Spectra and Radiative Transitions*, 2nd ed. New York: Springer, 1992.

48 D. A. Steck. "Cesium D line data," *available online at* http://steck.us/alkalidata *(revision 2.1.4, 23 December September 2010)*, 2010.

49 D. A. Steck, "Rubidium 85 D line data," *available online at* http://steck.us/alkalidata *(revision 2.1.6, 20 September 2013)*, 2013.

50 C. L. Holloway, M. T. Simons, M. Kautz, P. F. Wilson, and J. A. Gordon, "Development and applications of a fiber-coupled atom-based electric field probe," in *2018 International Symposium on Electromagnetic Compatibility (EMC Europe 2018), Amsterdam, The Netherlands, Aug 27–30*, pp. 381–385, 2018.

51 W. Demtröder, *Atoms, Molecules and Photons: An Introduction to Atomic-, Molecular-, and Quantum Physics*, 2nd ed. New York: Springer, 2010.

52 M. T. Simons, A. B. Artusio-Glimpse, C. L. Holloway, E. Imhof, S. R. Jefferts, R. Wyllie, B. C. Sawyer, and T. G. Walker, "Continuous radio frequency electric-field detection through adjacent Rydberg resonance tuning," *Phys. Rev. A*, vol. 104, 032824, 2021.

53 D. A. Anderson and G. Raithel, "Continuous-frequency measurements of high-intensity microwave electric fields with atomic vapor cells," *Appl. Phys. Lett.*, vol. 111, 053504, 2017.

54 H. Friedrich, *Theoretical Atomic Physics*, 4th ed. New York: Springer.

55 M. T. Simons, M. D. Kautz, J. A. Gordon, and C. L. Holloway, "Uncertainties in Rydberg atom-based RF E-field measurements," in *2018 International Symposium on Electromagnetic Compatibility (EMC Europe 2018), Amsterdam, The Netherlands, Aug 27–30*, pp. 381–385, 2018.

56 H. Fan, S. Kumar, J. Sheng, J. P. Shaffer, J. A. Gordon, and C. L. Holloway, "Effect of vapor-cell geometry on Rydberg-atom-based measurements of radio-frequency electric fields," *Phys. Rev. Appl.*, vol. 4, 044015, 2015.

57 J. P. Shaffer, "Atom-based electromagnetic field sensing," *SPIE 11296, Optical, Opto-Atomic, and Entanglement-Enhanced Precision Metrology II, 27 March 2020*, https://doi.org/10.1117/12.2552626, 2020.

58 H. Mu, H. Zou, Q. Wang, and Z. Song, "A low permittivity metamaterial on a glass substrate for fabricating an atomic vapor cell," *2019 Photonics & Electromagnetics Research Symposium - Fall (PIERS - Fall), Xiamen, China, 2019*, pp. 344–350, 2019. doi: 10.1109/PIERS-Fall48861.2019.9021792.

59 M. T. Simons, A. H. Haddab, J. A. Gordon, and C. L. Holloway, "Applications with a Rydberg atom-based radio frequency antenna/receiver," *2019 International Symposium on Electromagnetic Compatibility (EMC Europe 2019), Barcelona, Spain, Sept 2–6*, pp. 885–889, 2019.

60 D. A. Anderson, R. E. Sapiro, and G. Raithel, "Rydberg atoms for radio-frequency communications and sensing: Atomic receivers for pulsed RF field and phase detection," *IEEE Aerospace Electron. Syst. Mag.*, vol. 35, no. 4, pp. 48–56, 2020.

61 S. Ottoa, M. K. Hunter, N. Kjærgaard, and A. B. Debb, "Data capacity scaling of a distributed Rydberg atomic receiver array," *J. Appl. Phys.*, vol. 129, 154503, 2021.

62 M. T. Simons, A. B. Artusio-Glimpse, A. K. Robinson, N. Prajapati, and C. L. Holloway, "Rydberg atom-based sensors for radio frequency electric field metrology, sensing, and communications," *XXIII IMEKO World Congress: Measurement: Sparking Tomorrow's Smart Revolution, Yokohama, Japan, Sept 2021*, 2021.

63 D. A. Anderson, G. Raithel, M. T. Simons, and C. L. Holloway, "Quantum-optical spectroscopy for plasma electric field measurements and diagnostics," *arXiv:1712.08717v1 [physics.atom-ph], Dec 23*, 2017.

64 E. B. Norrgard, S. P. Eckel, C. L. Holloway, and E. L. Shirley, "Quantum blackbody thermometry," *New J. Phys.*, vol. 23, 033037, 2021.